Nucleic Acids Research, 1996, Vol. 24, No. 2 321–329

Visualization and analysis of unfolded nucleosomes associated with transcribing chromatin

David P. Bazett-Jones*, Elizabeth Mendez[1,+], Gregory J. Czarnota[2], F. Peter Ottensmeyer[2] and Vincent G. Allfrey[1]

Departments of Anatomy and Medical Biochemistry, The University of Calgary, Calgary, AB, T2N 4N1, Canada, [1]Laboratory of Cell Biology, Rockefeller University, New York, NY 10021, USA and [2]Department of Medical Biophysics, University of Toronto, and Ontario Cancer Institute, 500 Sherbourne Street, Toronto, ON, M4X lK9, Canada

Received September 15, 1995; Revised and Accepted November 26, 1995

ABSTRACT

We have characterized the structure of transcriptionally active nucleosome subunits using electron spectroscopic imaging. Individual nucleosomes were analyzed in terms of total mass, DNA and protein content, while the ensemble of images of active nucleosomes was used to calculate a three-dimensional reconstruction. Transcriptionally active nucleosomes were separated from inactive nucleosomes by mercury-affinity chromatography thus making it possible to compare their structures. The chromatographic results combined with electron spectroscopic imaging confirm that active nucleosomes unfold to form extended U-shaped particles. Phosphorus mapping indicated that the nucleosomal DNA also underwent a conformational change consistent with particle unfolding. The three-dimensional structure of the Hg-affinity purified nucleosomes determined using quaternion-assisted angular reconstitution methods unites and resolves the different electron microscopic views of the particle and is concordant with a sulphydryl-exposing disruption of the H3–H4 tetramer.

INTRODUCTION

The canonical conformation of the nucleosome particle, as determined by X-ray crystallographic analysis of nucleosomes from transcriptionally quiescent genes, is a disc, 110 Å in diameter and 57 Å in height (1–3). Its centre is a wedge-shaped protein octamer containing two each of the histones H2A, H2B, H3 and H4, around which 146 bp of DNA are wound in 1.8 negative superhelical turns. The X-ray structure of the octameric protein core shows a centrally located $(H3–H4)_2$ tetramer which contains buried sulphydryls, flanked by two H2A–H2B dimers (4). The three subunits are assembled in the form of a left-handed protein super helix, with a pitch of 28 Å and form a solid object with a small central cavity. A distribution of positive charges on the surface of the octamer appears as a left-handed spiral at the calculated path of the DNA. A model of the nucleosome core particle, based on this data, shows that the two DNA strands coincide with the path of the histone positive charges, and that the central 12 turns of the DNA double helix contact the surface of the octamer at repetitive structural motifs (5). Contacts between the individual histones and the encircling DNA have been mapped by chemical cross-linking experiments (6,7). Histones H3 and H4 are cross-linked to DNA within 30 bp on either side of the dyad axis. Histones H2A, H2B and H3 are cross-linked to the DNA where it enters and exits the nucleosome. Both chemical (7) and UV-laser cross-linking methods (8) show that the N-terminal domains of the histones make numerous contacts with the DNA coil at the periphery of the nucleosome (9). The cysteine residues of the two histone H3 molecules lie within a few Angstroms of each other at the centre of the core, where they are not accessible to SH-reactive agents (10).

This compact structure would be expected to restrict the accessibility of DNA to RNA polymerases and transcription factors. Although most transcriptionally active genes are packaged into nucleosomes, they are organized into a less condensed chromatin structure. This is achieved in part by a depletion of histone H1 (11), which normally binds the DNA strand where it enters and exits from the nucleosome core, and by a relaxation of histone-imposed constraints on DNA within the core particle. Active regions of chromatin are highly accessible to hydrolytic cleavage by DNase I (12,13), DNase II (14,15), and micrococcal nuclease (16,17). Moreover, the sensitivity of a gene to micrococcal nuclease (MNase) is related to the timing of its transcription. The MNase-sensitive domain does not include the non-transcribed DNA sequences flanking the gene, and this sensitivity is lost when transcription stops (16,17). On the chemical level the individual histone proteins become hyperacetylated in their N-terminal regions, resulting in a number of transcriptionally-associated changes in physico-chemical properties (18–20).

Whereas it is recognized that changes in DNA topology and altered histone–DNA contacts occur in active chromatin, the corresponding structural basis for conformational changes of the nucleosome has not yet been fully addressed. Elongated forms of the nucleosome core believed to be associated with transcrip-

* To whom correspondence should be addressed

+Present address: Department of Embryology, Carnegie Institute of Washington, 115 W. University Pkwy, Baltimore, MD 21210-3399, USA

tional activity have been detected by electron microscopy (21). Similarly, nucleosomes from transcribing ribosomal genes of *Physarum* seem to be unfolded into a so-called lexosome structure stabilized by non-histone proteins (10).

Since transcriptionally active nucleosomes can be separated specifically from inactive particles by mercury-affinity chromatography, it is possible to analyze the active structure in two and three dimensions without interference from inactive chromatin fragments (22–25). To characterize the structure of nucleosomes associated with transcriptionally active genes, we have chosen to use electron spectroscopic imaging (ESI), a technique that permits high resolution structural studies and elemental microanalysis (26–32). An advantage of this technique is its ability to quantify the characteristics of individual nucleosomes, specifically their total mass, DNA and protein contents. Moreover, it can be anticipated that structural changes will alter the path of the DNA within the nucleosome. The ability to map the phosphorus organization, and thereby the DNA path, makes ESI particularly sensitive for detecting alterations in nucleoprotein structure. Though ESI requires a high exposure of the specimen to the electron beam, the stability of DNA–protein complexes that have been so analyzed permits the collection of images that have resolution in the 10–20 Å range (29,32). Other high resolution methods for studying highly modified nucleosome particles that can provide such information are not currently available.

Following ESI, the three-dimensional structure of nucleosomes associated with transcriptionally active genes was determined using image processing methods based on quaternion-assisted angular reconstitution. This technique permits the three-dimensional structures of biological macromolecules to be calculated from randomly oriented particles (33–37). The results of Hg-affinity chromatography combined with this microscopical analysis confirm that active nucleosomes are unfolded, forming extended U-shaped particles, consistent with a disruption of the H3–H4 tetramer. The changes in nucleosome conformation are consistent with a model where only unfolding occurs, with no additional requirement for displacement of the histone core (38).

MATERIALS AND METHODS

Preparation of Chromatin

COLO 320 DM cells, human adenocarcinoma cells (obtained from ATCC), were grown in DMEM supplemented with 10% newborn calf serum (Gibco), 100 µg/ml penicillin, 100 µg/ml streptomycin, 10 µg/ml gentimycin sulphate (Gibco). The cells were harvested in log phase at a concentration of 10^5 cells/ml. Nuclei were prepared as described (24), and nucleosomes were released by a limited digestion with micrococcal nuclease. To minimize further degradation of the unfolded monomers (24), conditions were modified to release only 3–5% of the total nuclear DNA into the S1 fraction. The released chromatin fragments were fixed in 1% buffered, EM grade formaldehyde for 5 min at room temperature in 50 mM Tris–HCl, 50 mM NaCl, 0.5 mM $MgCl_2$, 1 mM β-mercaptoethanol and 5 mM sodium butyrate and immediately applied to a mercury-affinity column. After washing the column to elute the unbound nucleosomes, the Hg bound nucleosomes were eluted in two steps, as described (24). Two samples of each nucleosome fraction were submitted for electron spectroscopic imaging. One was not further treated, whereas the other was treated with 50 µg/ml RNase A for 1 h at 37°C. All samples were then dialyzed against a buffer of 10 mM Tris–HCl, 1 mM EDTA pH 8.0 at 4°C, and imaged by ESI.

Mass and phosphorus analysis of nucleosome particles by ESI

Nucleosomes fractionated by a 2-step Hg-affinity chromatography procedure were spread onto a 2–3 nm-thick carbon support film supported on 1000-mesh copper grids. The carbon films were exposed to glow discharge immediately before use. Linearized plasmid DNA was spread with the nucleosomes to serve as an internal reference for both mass and phosphorus analyses (27,32). A 4 µl drop of nucleosomes and a 4 µ1 drop of DNA solution were applied together to the grid. The total concentration of the chromatin and DNA was ~20 µg/ml. If necessary, a final dilution on the grid surface was carried out by injection of an equal volume of buffer into the chromatin/DNA droplet on the grid surface. After 30 s the grid was washed with buffer to remove excess, unbound sample, followed by a wash with distilled H_20. Excess was removed with filter paper, after which the specimen was air dried.

To provide a dose-sparing darkfield-like image, grids were examined at about 30 eV energy loss. Phosphorus-enhanced images were recorded by imaging with electrons corresponding to the phosphorus ionization peak at 155 eV energy loss. Reference images were recorded before the phosphorus edge at energy losses of 105 and 120 eV. Micrographs were recorded on Kodak SO-163 electron image film at a magnification of 13 000 or 20 000 ×. The film was developed for 10 min in full-strength Kodak D-19 developer. Micrographs were digitized on a computerized image capture system and analyzed (39). The digitized pixel size corresponded to 10 µm on the film, permitting a number of nucleosomes to occupy a field, usually also with a portion of a molecule of control DNA. Background regions were used to normalize the reference and the phosphorus-enhanced images in order to offset slight differences in micrograph exposure density. Differences greater than 10% resulted in rejection of the image sets to avoid potential non-linearity problems between the films. In order to delineate the objects, the average background value was chosen as a threshold for the reference and phosphorus enhanced images. Objects were then outlined interactively and the integrated optical densities were calculated. The integrated optical density of an object is relatively insensitive to the size of the delineation mask in this procedure. An integrated optical density of a nucleosome and a defined length of linearized plasmid DNA are both obtained from the 120 eV reference image which is essentially a ‘mass’ image, obeying Beer’s law. Knowing the length of the DNA and its molecular weight and assuming an average molecular mass of 650 Da per base pair and an experimentally determined value of 3.4 Å/bp, the integrated optical densities were converted to mass, so that by comparison, the mass of the nucleosomes could be estimated. The same masks, for the standard DNA and for the nucleosomes, were then used to calculate the phosphorus content of the same nucleosomes in the net phosphorus images (39). To calculate the mass and phosphorus content on either side of an apparent plane of symmetry in the Hg-affinity column bound fraction, masks were created on both sides of the chosen plane. To determine the symmetry plane, the particle boundary was delineated at a background value plus one standard deviation measured over the background. The two longest axes were drawn by hand using a mouse and a line joining the midpoints of these lines or a line

orthogonal to it at its midpoint formed the axis of symmetry. In some cases the line through the bisection of the angle at the point of intersection of the two longest axes created a symmetry axis. To minimize error from the determination of this plane, average values of mass and phosphorus were obtained by moving the line ~10 Å to either side of the chosen plane.

Three-dimensional image processing

Three-dimensional reconstructions were calculated using an approach based on quaternion-assisted angular reconstruction (33–37). The method permits the three-dimensional reconstruction of biological macromolecules and their complexes from sets of images of single particles at random orientations. It has been used to determine the three-dimensional structures of proteins (35,36). Using ESI images of the nucleosome purified from inactive chromatin fractions, the method has been applied to calculate the three-dimensional structure of different conformational states of the particle with respect to different ionic environments (40). In the current study, ESI images of Hg-affinity purified nucleosomes were selected on the basis of their molecular mass. Outliers with a mass of more than one standard deviation from the mean were excluded. In order to obtain images with a higher signal to noise ratio, three-dimensional image processing was carried out using the phosphorus contrast enhanced images acquired at 155 eV energy loss. Three-dimensional reconstructions were calculated as before (35,36). The quaternion-assisted angular reconstitution approach (36) is based upon the principle of common lines (37). This principle states that projection images of a particular macromolecule at different orientations share common lines of integrated intensity. By determining these common lines it is possible to determine the relative angular orientations amongst many projection images. The method is robust, has been tested with simulated images and a macromolecule of known structure and in protein structure determination (34–36).

In the reconstruction process, 150 nucleosome images were used. This is a greater than sufficient number to permit 3D reconstructions to be calculated at high signal-to-noise ratios and at resolutions of 15–30 Å, which permit gross nucleosome conformation to be determined (36). To determine the resolution, the set of 150 images was split randomly into two sets of 75 images and two independent reconstructions were determined. A phase residual approach was used to determine the level of consistency between the two reconstructions, a measure of resolution. A phase residual based approach provides a measure of average structural overlap at particular spatial frequencies and is effectively a consistency measure between features of specific sizes in the reconstructions. This method and comparisons to other methods is extensively discussed elsewhere (36). At a phase residual of 60°, a conservative measure of average overlap or resolution, the reconstructions correlated to 30 Å. At a phase residual of 90°, the point at which average overlap no longer occurs, the reconstructions correlated to 18 Å. This latter measure is equivalent to the Fourier ring correlation with a cut-off at two standard deviations of the noise. These numbers are consistent with other studies carried out using the quaternion-assisted angular reconstruction approach (36,40).

RESULTS

The ability to separate transcriptionally active from inactive nucleosomes by mercury affinity chromatography makes it possible to compare their structures without the confounding characteristics inherent in a mixture of active and inactive chromatin fragments.

Typical conformations of the nucleosomes in the Hg column flow-through and the DTT eluted fractions imaged in energy loss mode are shown in Figure 1. The length:width ratios of the particles show that nucleosomes of the mercury-bound fractions are considerably extended relative to the compactly beaded nucleosomes of the unbound fraction (Table 1). The length:width ratios of the nucleosome fractions eluted in 0.5 M NaCl and in 20 mM DTT, relative to the unbound nucleosomes, are compatible with an unfolding mechanism that involves a relaxation of constraints on the DNA coiled around the histones of the nucleosome core. This view is supported by the differences in morphology of the particles from the unbound and Hg-bound fractions.

Virtually all of the nucleosomes of the unbound fraction (~88%) resemble compact toroids, with an average mass of 208 kDa, whereas only 7% display a U-shaped or elongated outline, and 5% appear as distorted or 'swollen' circular profiles. ESI analysis of particles with an average of 162 ± 28 bp of DNA gave an average total protein content of 101 ± 29 kDa (Table 1). A plot of the estimates of protein content versus DNA content (Fig. 2A) is consistent, within the measurement errors, of nucleosomes in their canonical conformation. In agreement with the results of X-ray crystallography (4,5), ESI also reveals that the compact nucleosomes have a central cavity or region of lower mass density (Fig. 1A).

The nucleosomes released from the mercury-column in 0.5 M NaCl were not all compactly beaded (not shown). Instead their images revealed a mixture of three classes of chromatin subunits: (i) approximately 27% resembled toroids (circular profiles with reduced mass in the centre); (ii) 50% had U-shaped or elongated profiles; and (iii) 23% had a distorted or 'swollen' circular profile with a diameter 10–20% greater than the toroids of the unbound fraction but without reduced mass in the centre. The expanded state of this Hg-bound nucleosome is not surprising, in light of the evidence that all thio-reactive nucleosome fractions have consistently shown very high levels of histone acetylation (22–25,41–43) and that hyperacetylation weakens and shifts histone–DNA interactions at the centre of the nucleosome core (8,44). Most of the U-shaped particles of the 0.5 M NaCl wash fraction have DNA contents in the range expected for mononucleosomes of COLO320 cells (average = 158 bp) (Fig. 2C). They exhibit, however, a larger spread in the protein mass distribution in comparison to control nucleosomes (Fig. 2C), and the average protein mass, 88 kDa, falls below that expected for a complete histone octamer (108 kDa).

We are confident that the elongated or U-shaped profiles are not the result of exposure to 0.5 M NaCl. First, the exposure of the particles to fixative before the chromatography should prevent unfolding. Nevertheless, to test whether 0.5 M NaCl alone could lead to a detectable disruption of the canonical structure, we exposed a sample of the pre-fixed, flow-through nucleosome fraction to 0.5 M NaCl. The appearance of these particles in the subsequent ESI analysis was indistinguishable from the same fraction not exposed to this salt concentration (Fig. 1C). We conclude, therefore, that the elongated or U-shaped appearance of the column bound, salt eluted fraction is not due to exposure to 0.5 M NaCl.

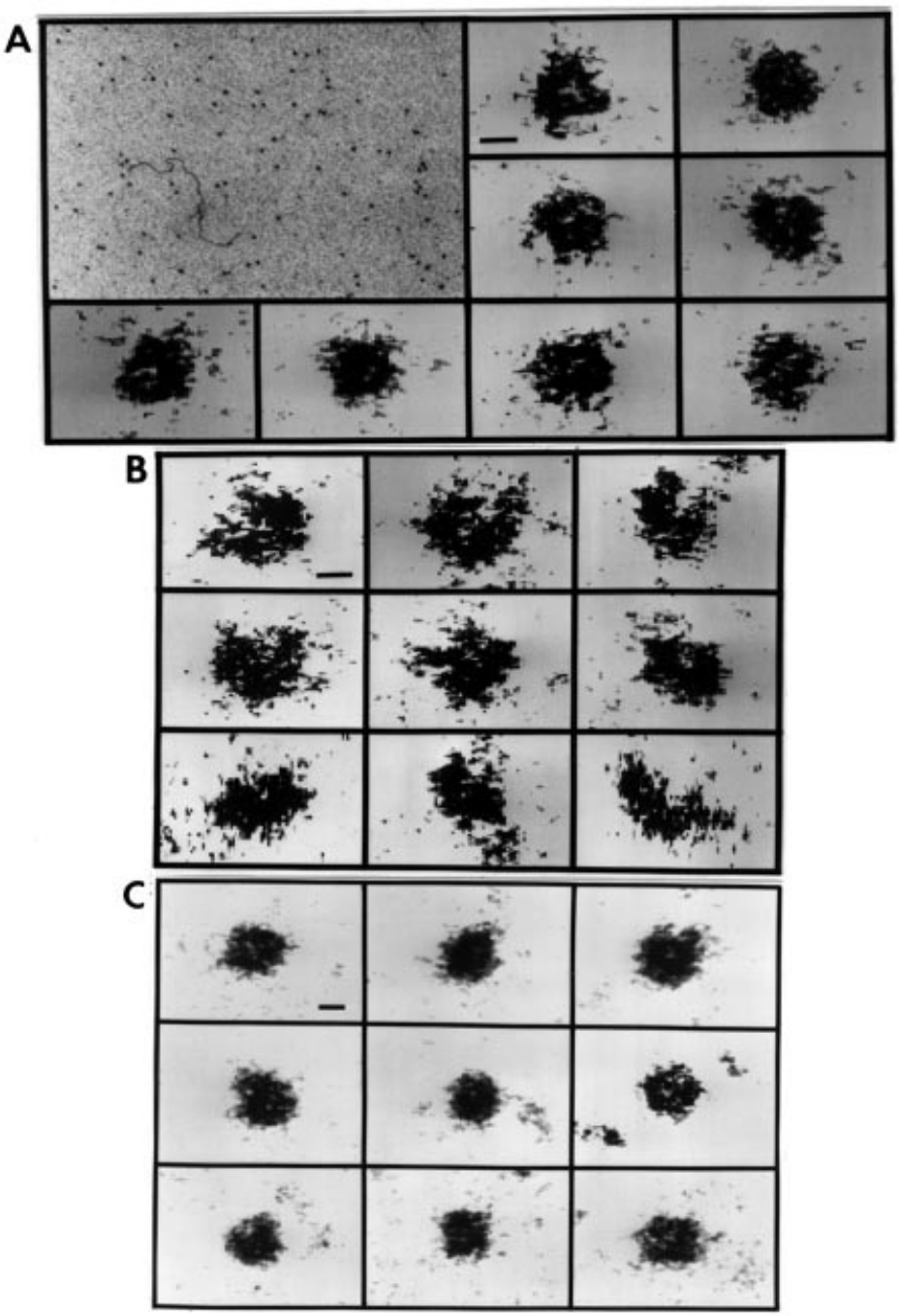

Figure 1. Electron spectroscopic images of nucleosome particles from (**A**) the flow-through fraction, (**B**) the DTT-eluted fraction of the Hg-affinity chromatography column, (**C**) the flow-through fraction exposed to 0.5 M NaCl before ESI analysis. The field view in (A) shows a DNA fragment used as a standard for estimating mass and DNA content of particles. All of the particles shown at higher magnification are represented in this field. The field view was recorded at 155 eV energy loss whereas the higher magnification views in (A), (B) and (C) were recorded at an energy loss of 120 eV. Scale bar represents 120 nm in the field view and 4.8 nm in the high magnification images.

Unfolded particles were even more prevalent in the DTT-eluted nucleosome fraction eluted with one step, without exposure to 0.5 M NaCl. Approximately 62% of the particles were elongated or U-shaped (Fig. 1B). Conversely, only 13% of the DTT-eluted fraction appeared toroidal and 25% had a distorted or 'swollen' profile. The presence of the U-shaped nucleosomes in the DTT-eluted fraction is of particular interest, since that fraction consists only of nucleosomes linked to the Hg-column through accessible thiols of histone H3 (24,43). It is not necessary, therefore, for the nucleosome to unfold completely to reveal the H3-thiol groups known to be located at the centre of the core (10). Again, we argue that it is not likely that either the nuclease digestion or column buffers are responsible for the unfolded appearance of the column-bound fractions for the following

Table 1.

Table 1	Mean Length:Width Ratio ± 1 s.d.	Average DNA Content (bp) ± 1 s.d.	Average Protein Content (kD) ± 1 s.d.	Average Total Mass (kD)	Average Mass Fraction DNA on ◇high mass side ± 1 s.d.	Average Mass Fraction DNA on ◇low mass side ± 1 s.d.
* Control	1.15 ± 0.07	162 ± 28 (n=96)	101 ± 29	208	0.50 ± 0.08 (n=30)	0.47 ± 0.07
+ DTT	1.67 ± 0.15	155 ± 40 (n=100)	111 ± 28	212	0.47 ± .18 (n=24)	0.60 ±0.17
+ NaCl	1.54 ± 0.11	158 ± 25 (n=95)	88 ±34	192	--	--

*Control, Flowthrough of Hg affinity chromatography column.
+DTT,NaCl, Fraction eluted with DTT or NaCl from Hg affinity chromatography column.
◇, Total mass measured on either side of mirror plane of symmetry in order to designate high or low mass side of the particles. On average, the DNA content on each side was equal within the measurement error.

reasons. First, the nuclease digestion buffer has an ionic strength close to the physiological level. Secondly, fixation before the Hg column would make further subsequent disruptions unlikely. And thirdly, even if the column buffer (10 mM Tris, 25 mM NaCl, 25 mM KCl, 2% sucrose, 5 mM sodium butyrate) was capable of causing a structural transition, exposure to it did not unfold the control fraction nucleosomes. They were compact, whereas the column-bound nucleosomes were elongated. Because the bound and unbound fractions were treated identically, the different appearance of particles in these fractions indicates an underlying structural difference and is not due to exposure to particular buffers or to other steps in the imaging process. Estimates of the DNA and protein content of the particles in this bound fraction revealed an average DNA content of 155 ± 40 bp and a protein content of 111 ± 28 kDa (Fig. 2B).

A three-dimensional reconstruction for the DTT eluted nucleosomes (Fig. 3) reveals an open or U-shaped conformation. The central core region of the nucleosome, normally inaccessible as indicated by X-ray crystallography (4,5), is open and accessible in this three dimensional reconstruction. This is consistent with biochemical observations of internal sulphydryl accessibility in nucleosomes associated with transcriptionally active genes. One half of the reconstruction also appears more massive than the other, consistent with mass measurements of individual nucleosomes given below. This is evident in the lower portion of the reconstruction shown in Figure 3. Profiles of the reconstruction are consistent with the images showing U shaped and extended projections.

The reconstruction described here was determined using 150 images of nucleosomes selected on the basis of their relative molecular mass. Two additional reconstructions were calculated from independent sets of 75 images. The 75-image reconstructions were similar to the 150-image reconstruction, appearing U-shaped and elongated (not shown). The use of a phase residual based approach, a measure of structural overlap, to compare these two reconstructions indicated a resolution of 30 Å at a phase residual of 60°, a conservative measure of resolution. This approach also indicated a resolution of 18 Å at a phase residual of 90°, the limit at which structural detail exhibits zero overlap. A more detailed discussion of these measures is given in reference 36.

A reconstruction has not yet been calculated for the particles of the flow-through eluate of the column, which corresponds to transcriptionally inactive nucleosomes. A reconstruction of transcriptionally inactive nucleosomes from calf thymus nuclei has been calculated, indicating a closed compact structure, consistent with the crystallographic form of the macromolecular complex (40). We have, however, compared length:width measurements and principle component analysis (45) results of the flow through fraction and calf thymus-derived nucleosomes. Both populations are nearly indistinguishable in the correspondence of their projections to that of an oblate ellipsoid (data not shown). We, therefore, expect that the reconstruction of the flow-through fraction will be similar to that of the calf thymus nucleosomes, indicating a closed, compact structure.

ESI permits the visualization of the phosphorus distribution in nucleosome particles, from which the path of the DNA can be inferred (Fig. 4) (29). Particles with high length:width ratios, such as those seen in Figure 1B, always show an extended DNA distribution. Because of the variety of projections that are possible, even particles with a lower length:width ratio can have a DNA distribution that indicates an unwinding of the supercoil. In some of the images, the DNA profile is U-shaped (Fig. 4A, rows 1 and 2). Phosphorus maps of many of the more elongated chromatin subunits strongly support the suggestion that the DNA around the U-shaped and elongated chromatin subunits has been stretched like the coil of a spring to form an S shaped projection of the DNA (Fig. 4A, rows 3 and 4). In this state, it is not surprising that the associated histone H3-thiol groups were readily accessible for binding to the Hg-column. As stated earlier, a small fraction of the particles have a compact circular profile similar to those in the control fraction. In fewer than one-third of these, the phosphorus or DNA appears to be confined to a trajectory at the periphery of the protein core (Fig. 4A, row 5), indistinguishable from those projections that were regularly observed with the control nucleosome particles (Fig. 4B).

To characterize these elongated particles further, we estimated the DNA and protein content of each half of a number of particles that had an apparent mirror plane of symmetry in the mass-sensitive images. The results are summarized in Table 1. Representative measurements made from images of individual nucleosomes are given in Table 2. The mass in each half of a nucleosome was

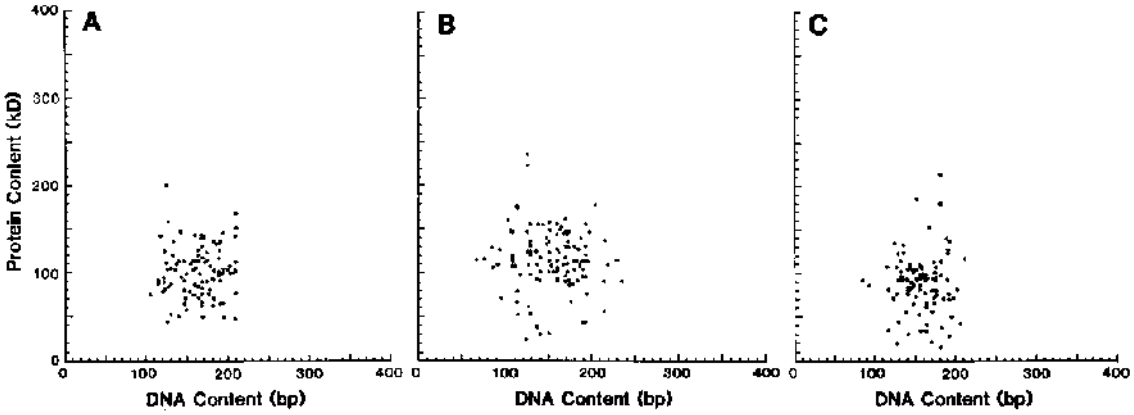

Figure 2. Scatter plots of measured protein content (kDa) versus DNA content (bp) of nucleosome particles imaged by ESI. The plots in A, B and C are derived from the particles in the flow-through, the DTT-eluted and the NaCl-eluted fractions, respectively, of the Hg-affinity chromatography column.

measured and designated as the high or low mass side. The phosphorus content of each half was measured. On average, the amount of DNA on each side was equivalent. In contrast, the ratio of the DNA to the protein mass on the low mass side of the Hg-bound particles, was ~20% higher than that on the high mass side. This indicates that a loss in protein may be the cause of the altered DNA to protein ratio on the low mass side. Variability was observed, however, between individual particles (Table 2). For example, the three particles analyzed in Table 2 each had 80 ± 5 bp DNA on each side of the mirror-symmetric plane. For particle 1, no significant difference in DNA to protein content from that obtained for control particles was observed on either side of the mirror-symmetric plane. For particles 2 and 3, however, there is a higher protein to DNA ratio on the high mass side and a lower protein to DNA ratio on the low mass side than that obtained for control particles. Since we cannot identify proteins with this analysis, we cannot determine whether altered protein to DNA ratios are due to altered core histone levels or to the presence of other factors. Electrophoretic analyses have shown that the Hg-bound nucleosomes contain all four histones in stoichiometric proportions (24,42,43). This, however, is a bulk property of all of the particles in the fraction. In contrast, the analysis presented in Table 2 indicates that variability in DNA:protein stoichiometry between individual particles and between symmetrical halves of particles is observed. But even this variability is not reflected in the average protein and phosphorus levels of the entire fraction nor would this variability be detectable in Coomassie-stained protein gels or gels to assay DNA length.

DISCUSSION

In this study we have shown that transcriptionally active nucleosomes isolated by Hg affinity chromatography are structurally dissimilar from the bulk fraction of nucleosomes that do not bind to the affinity column. The Hg-bound particles have a considerably larger length to width ratio than those that do not bind. They also often appear elongated or U-shaped in two dimensional images. The three-dimensional model calculated from electron micrographs of such particles indicates how the U-shaped and extended features are characteristics of a single structure at different orientations. Analysis of individual net phosphorus images indicates that the DNA, able to uncoil from a compact superhelix, can take on the appearance of a stretched spring. From the appearance of many of these particles and the accessible nucleosomal interior as revealed by the three-dimensional model, it is not surprising that the sulphydryls of the H3 histones are exposed and, therefore, bind to the Hg column. Mass and phosphorus estimates by ESI indicate that the bound particles on average are not depleted in protein or DNA content. This analysis, however, does not rule out the possibility that core histones can sometimes be replaced with non-histone chromosomal proteins. There is an indication from the analysis of single particles and from the three-dimensional model that protein can be displaced from one side of the mirror symmetry plane of the U-shaped particles. Though these differences can be detected in individual particles by ESI, the changes are not reflected in the bulk properties of the fraction, such as protein mass analysis of many particles or biochemical assays to detect DNA length (24) or histone stoichiometry (42,43).

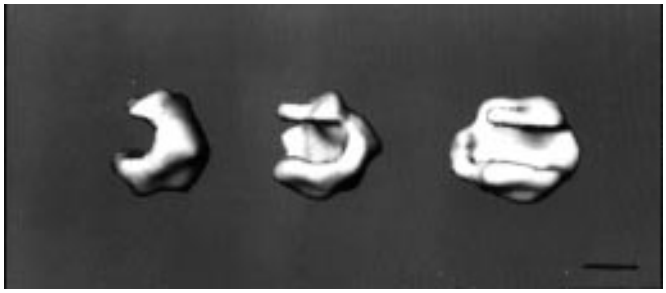

Figure 3. Three-dimensional reconstruction calculated from images of DTT-eluted nucleosomes associated with transcriptionally active genes. The three views from left to right are related to one another by sequential rotations of 45° to the right about a vertical axis in the plane of the page. The projection at the left shows a U-shaped conformation (on its side) whereas the open interior of the nucleosome is illustrated in the projection at the right. The lower part of the reconstruction is more massive than the other. Scale bar indicates 50 Å.

In considering the variety of nucleosome conformations made evident by ESI, and the distribution of the various forms in the unbound and Hg-bound fractions, it is important to recognize that binding of nucleosomes to a mercurated support is dependent upon transcription (22–25), and that the binding is eliminated within minutes after transcription is suppressed (25). It follows

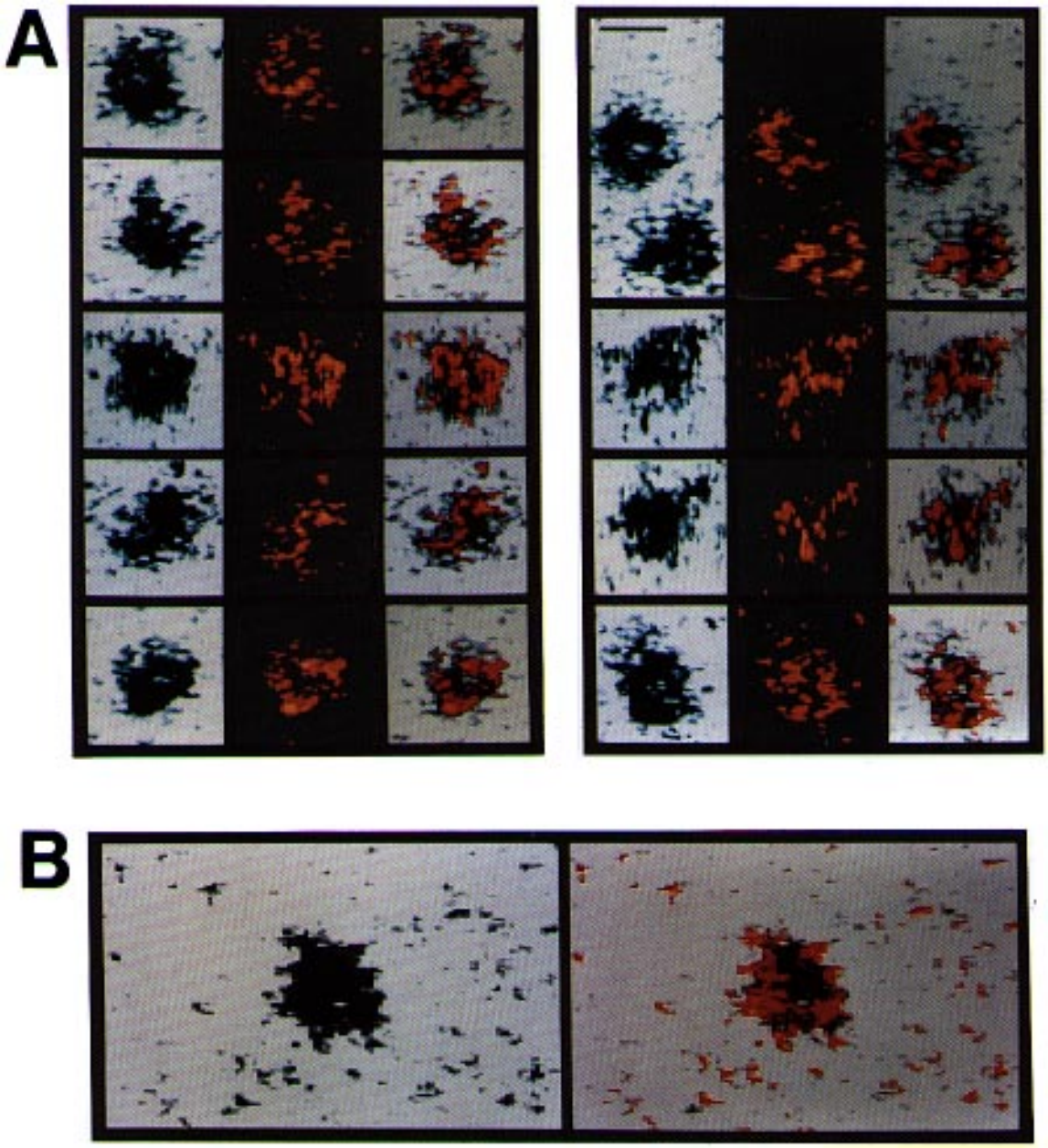

Figure 4. Electron spectroscopic images of nucleosome particles (**A**) from the DTT-eluted fraction and (**B**) from the flow-through fraction. In (A), a mass-sensitive image is shown (left), recorded at 120 eV energy loss, the net phosphorus image obtained from the subtraction of the 120 from the 155 eV image (centre), and the superposition of these two images (right). In (B), the mass image (left), and the superposition of the mass image and the net phosphorus image are shown (right). Scale bar represents 11 nm in A and 8.3 nm in B.

that the nucleosome core is a dynamic structure, changing its conformation and composition to facilitate (or hinder) transit of RNA polymerases along the template. This dynamic nature of the nucleosome is in accord with numerous genetic and biochemical studies which imply an active nucleosome structure (18,20). The compactly beaded particles of the unbound fraction clearly represent the nucleosome in its inactive state. That fraction contains the transcriptionally quiescent DNA of the cell (22–25). The rapid transitions between Hg-bound and unbound fractions that correlate with induction or repression of transcription indicates that an equally rapid mechanism must exist for relaxing the structural constraints on the DNA coil in the nucleosome. A capacity for the DNA to uncoil could facilitate the passage of RNA polymerase through the extended nucleosome particle. Without the ability to unfold in this way, a displacement of the nucleosomal histones from the DNA would likely be required for passage of the polymerase complex. The changes in nucleosome conformation reported here are consistent with a model where only unfolding occurs, with no additional requirement for the complete displacement of the histone core (38). Some nucleosomes displayed a lower than the canonical protein to DNA ratio on one side of the mirror symmetry axis coupled with a higher protein to DNA ratio on the other. This observation is consistent with a transient displacement of histone from one side to the other,

Table 2.

	High Mass Side		Low Mass Side	
Nucleosome	*Mass Fraction Whole Nucleosome	+Mass Fraction of DNA	*Mass Fraction of Whole Nucleosome	+Mass Fraction of DNA
1	0.56	0.51	0.44	0.50
2	0.52	0.44	0.48	0.58
3	0.55	0.36	0.45	0.64

*, The mass was measured on each side of a mirror plane of symmetry of three particles. The fraction of the mass on each side was calculated.
+, The mass fraction of DNA on each side was measured. The DNA content on each side was 80 ± 5 bp. The variation in mass fractionof DNA is due to variation in protein content on each side.

which may be required or result from polymerase passage. More frequently, however, the low mass side of the Hg-bound particles showed a higher DNA to protein ratio, indicating a loss of protein on one side of the particle. This may be the result of a loss of an H2A–H2B dimer from some particles.

The unfolded form of the nucleosome is likely not an artifact of the preparation, but reflects an unfolding mechanism *in situ*. The accessibility of H3-thiols in the transcribed regions of ribosomal genes was demonstrated in intact nucleoli (46). This accessibility is a clear indication that the nucleosome core has unfolded at its centre, and the energy loss images of the nucleosomes containing reactive H3-thiols present direct evidence that the unfolding involves more than a minor perturbation. Moreover, the unfolded state is not likely an artifact of preparation because only the nucleosomes along the transcribed sequences of the *Physarum* ribosomal genes have accessible H3-thiols, whereas nucleosomes along the non-transcribed central spacer are not thiol-reactive. Furthermore, the H3-thiol reactivity of the nucleosomes along the transcribed rDNA sequences is not observed when rDNA transcription is suppressed. These changes in H3-thiol reactivity are not accompanied by alterations in histone content, but they are reflected in levels of histone acetylation (46). Finally, in avian erythrocytes, the thiols of some nucleosomes can be labelled *in situ* (47), indicating that the exposure of these thiols is not a preparation artifact.

Comparisons of the current results with those of an earlier ESI study of hyperacetylated nucleosomes (28,29) lend support to the proposal that a rapid turnover of histone acetyl groups is a major factor in unfolding the nucleosome core for transcription. In these earlier studies, HeLa cells were cultured in the presence of sodium butyrate, an inhibitor of histone deacetylase (48–50), to induce the accumulation of the hyperacetylated forms of the core histones. A direct correlation was observed between the level of histone hyperacetylation and the extent to which nucleosomes lost their compact shape and became elongated. It is significant that the degree of elongation varied depending on the ionic strength of the buffers used in binding the hyperacetylated particles to the charged carbon support grids used for the electron microscopy. Marked differences in the length:width ratios between the hyperacetylated and control core particles observed at low ionic strength were not seen when the particles were bound to the carbon support at higher ionic strengths in the presence of Mg^{2+} ions. That study by ESI on the effects of ionic strength on nucleosome structure clarifies a number of confusing and often conflicting observations on the physical properties of hyperacetylated nucleosomes (51–53). It indicates that the unfolding promoted by hyperacetylation would not be extensive *in vivo* (i.e. at physiological ionic strengths) and may require the participation of other factors. Other histone modifications, such as phosphorylation, may contribute to this destabilization. Alternatively, or in addition, an increase towards positive DNA superhelicity ahead of the elongating polymerase may work together with histone acetylation to destabilize the particle. Thus, the underlying lowered stability of the hyperacetylated core particles would be a necessary but not a sufficient component of the mechanism for unfolding the nucleosome for transcription. In some contexts, maintenance of the unfolded state may also require other protein factors. Non-histone chromosomal proteins are known to be present in the Hg-column bound fractions (31,39–41). Or, the maintenance of the unfolded state may require other histone modifications. For example, the ubiquitination of histone H2B is transcription-dependent (54). Such a modification occurring simultaneously with elongation of the nucleosome may temporarily fix the particle in an unfolded state.

In another study, ESI analysis of a salt-soluble fraction of chicken erythrocyte chromatin, showing a 48-fold enrichment of the β-globin gene, demonstrated the presence of elongated nucleosome particles (55). The nucleosomes from this fraction were classified as having a circular profile (66% of the total), or a U-shape (22% of the total). Particles with a circular profile had a total mass of 205 kDa and contained 146 bp of DNA. This type of particle, resembling the canonical nucleosome core in shape and composition, was also the predominant type in the bulk chromatin (88% of the total) and probably originated mainly from non-transcribed genes. The U-shaped particles had a total mass of 170 kDa and contained 135 bp of DNA. They appeared almost exclusively in the salt-soluble fraction along with more elongated nucleoprotein structures of similar composition and correlate with high levels of acetylation, ubiquitination of H2B and depletion of H1 (reviewed in 55). The presence of these elongated forms in a chromatin fraction enriched in transcriptionally competent genes strongly indicates that they represent the active or poised state of the nucleosome. That interpretation is now supported directly by the structural characterization of the particles separated by Hg-affinity chromatography reported in this study, which have also been shown to contain high levels of acetylated core histones (24).

The lability of an H2A–H2B dimer has been indicated to be a characteristic of transcriptionally active nucleosomes (56). Disruptions that affect the H3–H4 tetramer in such particles, however, in other structural and biochemical data, are supported

by this study as well. Micrococcal nuclease digestion of the rDNA chromatin of *Physarum* releases two types of nucleosomes that can be separated by sucrose density-gradient centrifugation (10). The denser nucleosomes originate from the non-transcribed spacer, whereas the more slowly sedimenting nucleosomes are derived from the transcribed regions. These elongated and often bipartite 'A' particles are hyperacetylated and are fully accessible to SH-reagents, whereas the sulphydryls of H3 histones from the spacers are not available. Evidence for the existence of DNase 1-sensitive split or half-nucleosomes *in vivo* in yeast has been obtained (57). Disruption of nucleosomes on the hsp82 gene toward the 3′ end of the gene correlates with basal levels of transcription by engaged RNA polymerase II molecules. The transient positive supercoiling ahead of an elongating RNA polymerase may be partly responsible for the nucleosome splitting. Finally, exchange of all of the core histones, not just H2A and H2B, from salt-soluble, transcriptionally active/competent chromatin has been observed (58). Exchange of H3 and H4 is consistent with the present study, where U-shaped (in 2-D) and centrally cleft particles (in 3-D) derived from sulphydryl accessible, Hg-column bound nucleosomes, appear to have a disrupted H3–H4 tetramer.

ACKNOWLEDGEMENTS

We thank Manfred Herfort and Marjorie Louissaint for expert technical assistance. We thank Dr Michael J. Hendzel for his critical reading of the manuscript. The work was supported by research operating grants to FPO and DB-J from the Medical Research Council of Canada, an operating grant to FPO from the National Cancer Institute of Canada with funds from the Canadian Cancer Society, and an NIH research grant #CA-14908 to VGA. GJC is a recipient of a Steve Fonyo Scholarship from the National Cancer Institute of Canada. DPB-J was a scholar of the Alberta Heritage Foundation for Medical Research.

REFERENCES

1 Finch, J.T., Lutter, L.C., Rhodes, D., Brown, R.S., Rushton, B., Lewitt, M., and Klug, A. (1977) *Nature* **269**, 29–36.
2 Richmond, T.J., Finch, J.T., Rushton, B., Rhodes, D., and Klug, A. (1984) *Nature* **311**, 532–537.
3 Struck, M.M., Klug A., and Richmond, T.J. (1992) *J. Mol. Biol.* **224**, 253–264.
4 Arents, G., Burlingame, R.W., Wang, B.-C., Love, W.E. and Moudrianakis, E.N. (1991) *Proc. Natl. Acad. Sci. USA* **88**, 10148–10152.
5 Arents, G., and Moudrianakis, E.N. (1993) *Proc. Natl. Acad. Sci. USA* **90**, 10489–10493.
6 Mirzabekov, A.D., Schick, V.V., Belyavsky, A.V. and Bavykin, S.G. (1978) *Proc. Natl. Acad. Sci. USA* **75**, 4184–4188.
7 Pruss, D. and Wolffe, A.P. (1993) *Biochemistry* **32**, 6810–6814.
8 Ebralidse, K.K., Hebbes, T.R., Clayton, A.L., Thorne, A.W. and Crane-Robinson, C. (1993) *Nucleic Acids Res.* **21**, 4734–4738.
9 Stefanovsly, V.Y., Dimitrov, S.I., Russanova, V.R., Angelov, D. and Pashev, I.G. (1989) *Nucleic Acids Res.* **17**, 10069–10081.
10 Prior, C.P., Cantor, C.R., Johnson, E.M. and Allfrey, V.G. (1980) *Cell* **20**, 597–608.
11 Kamakaka, R.T., Thomas, J.O. (1990) *EMBO J.* **9**, 3997–4006.
12 Izban, M.G., and Luse, D.S. (1991) *Genes Dev.* **5**, 683–696.
13 Weintraub, H., and Groudine, M. (1976) *Science* **193**, 848–856.
14 Garel, A., Zolan, M. and Axel, R. (1977) *Proc. Natl. Acad. Sci. USA* **74**, 4867–4971.
15 Gottesfeld, J.M. and Butler, P.J.G. (1977) *Nucleic Acids Res.* **4**, 3155–3175.
16 Bellard, M., Kuo, M.T., Dretzen, G., and Chambon, P. (1980) *Nucleic Acids Res.* **8**, 2737–2750.
17 Bloom, KS. and Anderson, J.N. (1978) *Cell* **15**, 141–150.
18 Turner, B.M. (1991) *J. Cell Sci.* **99**, 13–20.
19 van Holde, K.E. (1988) *Chromatin*. Springer Verlag, New York.
20 Grunstein, M., Durrin, L.K., Mann, R.K., Fisher-Adams, G. and Johnson, LM. (1992) In McKnight, S.L. and Yamamoto, K.R. (eds) *Histones: Regulators of Transcription in Yeast in Transcriptional Regulation*. Cold Spring Harbor Laboratory Press, Cold Spring Harbor, NY, pp. 1295–1315.
21 Oudet, P., Spadafora, C., and Chambon, P. (1977) *Cold Spring Harbor Symp. Quant. Biol.* **42**, 301–312.
22 Sterner, R., Boffa, L C., Chen, T.A. and Allfrey, V.G. (1987) *Nucleic Acids Res.* **15**, 75–91.
23 Allegra, P., Sterner, R., Clayton, D.F., and Allfrey, V.G. (1987) *J. Mol. Biol.* **196**, 379–386.
24 Walker, J., Chen, T.A., Sterner, R., Berger, M., Winston, F., and Allfrey, V.G. (1990) *J. Biol. Chem.* **265**, 5736–5746.
25 Chen, T.A., Sterner, R. Cozzolino, A., and Allfrey, V.G. (1990) *J. Mol. Biol.* **212**, 481–493.
26 Bazett-Jones, D.P., Locklear, L., and Rattner, J.B. (1988) *J. Ultrastruct. Mol. Struct. Res.* **99**, 48–58.
27 Bazett-Jones, D.P. and Brown, M.L. (1989) *Mol. Cell. Biol.* **9**, 336–341.
28 Oliva, R., Bazett-Jones, D.P., Mexquita, C., and Dixon, G.H. (1987) *J. Biol. Chem.* **262**, 17016–17023.
29 Oliva, R., Bazett-Jones, D.P., Locklear, L., and Dixon, G.H. (1990) *Nucleic Acids Res.* **18**, 2739–2747.
30 Bazett-Jones, D.P., and Ottensmeyer, F.P. (1981) *Science* **211**, 169–170.
31 Adamson-Sharpe, K.M., and Ottensmeyer, F.P., *J. Microsc.* **122**, 309–314.
32 Bazett-Jones, D.P., Leblanc, B., Herfort, M., Moss, T. (1994) *Science* **264**, 1134–1137.
33 Farrow, N.A. and Ottensmeyer, F.P. (1992) *J. Opt. Soc. Am. A.* **9**, 1749–1760.
34 Farrow, N.A. and Ottensmeyer, F.P. (1993) *Ultramicroscopy* **52**, 141–156.
35 Czarnota, G.J., Andrews, D.W., Farrow, N.A. and Ottensmeyer, F.P. (1994) *J. Struct. Biol.* **133**, 35–46.
36 Serysheva, I.I., Orlova, E.V., Chiu, W., Sherman, M.B., Hamilton, S.L. and van Heel, M. (1995) *Nature Struct. Biol.* **2**, 18–23.
37 Crowther, R.A., DeRosier, D.J., Klug, A. (1970) *Proc. R. Soc. London Ser. A.* **317**, 319–340.
38 van Holde, K.E., Lohr, D.E., Robert, C. (1992) *J. Biol. Chem.* **267**, 2837–2840.
39 Bazett-Jones, D.P. (1993) *Microbeam Anal.* **2**, 69–79.
40 Czarnota, G.J., Ottensmeyer, F.P. (1996) *J. Biol. Chem.* (in press).
41 Boffa, L C., Walker, J., Chen, T.A., Sterner, R., Mariani, M.R. and Allfrey, V.G. (1990) *Eur. J. Biochem.* **194**, 811–823.
42 Chen, T.A., Smith, M.M., Le, S., Sternglanz, R., and Allfrey, V.G. (1991) *J. Biol. Chem.* **266**, 6489–6498.
43 Chen, T.A. and Allfrey, V.G. (1987) *Proc. Natl. Acad. Sci. USA* **84**, 5252–5256.
44 Simpson, R.T. (1978) *Cell* **13**, 691–699.
45 Zabal, M.M.Z., Czarnota, G.J., Bazett-Jones, D.P., Ottensmeyer, F.P. (1993) *J. Microsc.* **172**, 205–214.
46 Prior, C.P., Cantor, C.R., Johnson, E.M., Littau, V.C., Allfrey, V.G. (1983) *Cell* **34**, 1033–1042.
47 Chan, S., Attisano, L., Lewis, P.N. (1988) *J. Biol. Chem.* **263**, 15643–15651.
48 Boffa, L.C., Vidali, G., Mann, R.S., Allfrey, V.G. (1978) *J. Biol. Chem.* **253**, 3364–3366.
49 Johnson, E.M., Sterner, R., Allfrey, V.G. (1987) *J. Biol. Chem.* **262**, 69343–69346.
50 Candido, E.P.M., Reeves, R., Davie, J.R. (1978) *Cell* **14**, 105–113.
51 Sealy, L., Chalkley, R. (1978) *Cell* **14**, 115–121.
52 Bode, J., Gomez-Lira, M., and Schroter, H. (1983) *Eur. J. Biochem.* **130**, 7–445.
53 Ausio, J., and van Holde, K.E. (1986) *Biochemistry* **25**, 1421–1428.
54 Davie, J.R., Murphy, LC. (1990) *Biochemistry* **29**, 4752–4757.
55 Locklear, L., Ridsdale, J.A., Bazett-Jones, D.P. and Davie, J.R. (1990) *Nucleic Acids Res.* **18**, 7015–7024.
56 Jackson, V. (1990) *Biochemistry* **29**, 719–731.
57 Lee, M.S. and Garrard, W.T. (1991) *EMBO J.* **10**, 607–615.
58 Hendzel, M.J., and Davie, J.R. (1991) *Biochem. J.* **273**, 753–758.